


Article

Identifying Changes and Their Drivers in Paddy Fields of Northeast China: Past and Future

Xuhua Hu ¹, Yang Xu ², Peng Huang ¹, Dan Yuan ³, Changhong Song ⁴, Yingtao Wang ⁵, Yuanlai Cui ¹ and Yufeng Luo ^{1,*} 

¹ State Key Laboratory of Water Resources Engineering and Management, Wuhan University, Wuhan 430072, China; 2020202060089@whu.edu.cn (X.H.)

² Inner Mongolia Water Conservancy Research Institute, Hohhot 010051, China

³ School of Remote Sensing and Information Engineering, Wuhan University, Wuhan 430079, China

⁴ Heilongjiang Water Conservancy Investment Group Co., Ltd., Harbin 150090, China

⁵ Heilongjiang Provincial Water Conservancy and Hydroelectric Power Investigation, Design and Research Institute, Harbin 150080, China

* Correspondence: yfluo@whu.edu.cn; Tel.: +86-27-68776585; Fax: +86-27-68772310

Abstract: Northeast China plays a crucial role as a major grain-producing region, and attention to its land use and land cover changes (LUCC), especially farmland changes, are crucial to ensure food security and promote sustainable development. Based on the Moderate Resolution Imaging Spectroradiometer (MODIS) data and a decision tree model, land types, especially those of paddy fields in Northeast China from 2000 to 2020, were extracted, and the spatiotemporal changes in paddy fields and their drivers were analyzed. The development trends of paddy fields under different future scenarios were explored alongside the Coupled Model Intercomparison Project Phase 6 (CMIP6) data. The findings revealed that the kappa coefficients of land use classification from 2000 to 2020 reached 0.761–0.825, with an overall accuracy of 80.5–87.3%. The proposed land classification method can be used for long-term paddy field monitoring in Northeast China. The LUCC in Northeast China is dominated by the expansion of paddy fields. The centroids of paddy fields gradually shifted toward the northeast by a distance of 292 km, with climate warming being the main reason for the shift. Under various climate scenarios, the temperature in Northeast China and its surrounding regions is projected to rise. Each scenario is anticipated to meet the temperature conditions necessary for the northeastward expansion of paddy fields. This study provides support for ensuring sustainable agricultural development in Northeast China.

Keywords: paddy field expansion; remote sensing; land use and land cover change; climate warming



Citation: Hu, X.; Xu, Y.; Huang, P.; Yuan, D.; Song, C.; Wang, Y.; Cui, Y.; Luo, Y. Identifying Changes and Their Drivers in Paddy Fields of Northeast China: Past and Future. *Agriculture* **2024**, *14*, 1956. <https://doi.org/10.3390/agriculture14111956>

Academic Editor: Xiuliang Jin

Received: 17 September 2024

Revised: 28 October 2024

Accepted: 30 October 2024

Published: 31 October 2024



Copyright: © 2024 by the authors. Licensee MDPI, Basel, Switzerland. This article is an open access article distributed under the terms and conditions of the Creative Commons Attribution (CC BY) license (<https://creativecommons.org/licenses/by/4.0/>).

1. Introduction

Land use and land cover change (LUCC) is considered the key factor in global environmental change, encompassing complex dynamics that arise from the interactions between natural and social systems across multiple temporal and spatial dimensions [1–3]. As the crucial connection between natural ecological processes and human activities [4], LUCC exerts direct influence on the surface material–energy cycle, the sustainable utilization of natural resources, and human socioeconomic development [5–7]. LUCC includes not only changes in land use types but also changes in land use management, such as irrigation and planting structure, which can affect the regional environment and even contribute to global climate change [8]. It is necessary to realize green and sustainable development in areas with rapid development, prominent human–land contradictions, and fragile ecological environments. To achieve this, it is essential to timely and accurately determine the surface land cover status, explore the land use change trends, and identify the driving factors [9].

It is important to pay attention to spatiotemporal changes in land use, especially in farmland, and future trends to ensure food security. The spatial distribution of rice

cultivation in China is characterized by an increase in the north and a decrease in the south, moving from the southwest to the northeast [10,11]. Southern China is predominantly mountainous, with a limited availability of flat arable land [12]. Additionally, the rapid pace of urbanization has led to the conversion of large areas of farmland into construction land [13]. Furthermore, initiatives such as returning farmland to forest land have also contributed to the gradual reduction in the area dedicated to rice cultivation in the region [14]. The northeast region is considered the breadbasket of China [15,16]. In recent years, the most significant change in land use patterns in Northeast China has been the rapid expansion of paddy fields. This shift, driven by a combination of factors such as policy support, technological advancements, and climate changes, has garnered widespread attention [17,18]. However, long-term monitoring has been insufficient. Changes in paddy fields prior to 2000 have been extensively studied [19,20]. Rice production in Northeast China has been developing rapidly since 1990 [19]. Between 1995 and 2015, land use transformation in Northeast China displayed several prominent features. These included a persistent expansion of cultivated land, a steady decline in forestland and grassland, the rapid growth in construction land, and a reduction in unused land [21]. Xin et al. [18] found that the rice cultivation area in the three northeastern provinces of China experienced a substantial increase of 3.68 million ha from 2000 to 2017. Liu et al. [16] analyzed LUCC in Northeast China at approximately decadal intervals without continuous observational analysis. These are scattered studies, with less analysis and attention to the spatial and temporal variability of long time series and their causes. However, previous research has reached a consensus regarding the substantial growth of paddy fields in Northeast China [18,22]. Rice cultivation is influenced by many factors, and earlier research has primarily concentrated on the impacts of temperature and precipitation changes on the distribution of paddy fields [16]. However, policy, economic, and technological reasons are also important factors affecting its development. Systematic analyses and summaries are still lacking.

Anticipating future changes in paddy fields is important for sustainable development and food security. Land use modeling examines future scenarios by analyzing the underlying mechanism of LUCC [23,24]. In the last few years, many analytical and geographic models have been used to evaluate LUCC, such as SLEUTH [25,26], genetic algorithms [27], Markov chain [28,29], Future Land Use Simulation [30], Artificial Neural Network [31], and cellular automata [32,33]. The effects of climatic factors on LUCC have not been analyzed from a scientific perspective. There is no quantitative analysis or systematic observations to support the potential expansion of paddy fields due to climate warming. At both regional and global scales, the link between climate change and rice production has been given insufficient focus [34]. Research on how paddy fields will evolve under future climate change in Northeast China remains limited.

The traditional acquisition of land area in China relies on a combination of ground surveys and comprehensive statistical methods to gather information. Ground surveys collect detailed data through field assessments, allowing researchers to evaluate land characteristics and usage. Additionally, statistical offices compile data from agricultural censuses and local surveys, which are then aggregated and analyzed to produce annual reports [35]. However, this method is heavily dependent on statistical data, resulting in significant lags in research findings, in addition to being time-consuming and labor-intensive, particularly when monitoring large areas. The emergence of Geographic Information System (GIS) technology has brought about significant advancements in monitoring and analyzing spatiotemporal changes in land use [36]. It has enabled the utilization of remote sensing data, which offers regional advantages and timeliness, as a crucial data source for this purpose [37,38]. Data with low spatial resolution are usually employed for land use classification at broad regional or global scales [10,39,40]. Tucker et al. [41] used NDVI data from NOAA/AVHRR to study LUCC in Africa. At the regional scale, data from Moderate Resolution Imaging Spectroradiometer (MODIS) and Landsat are commonly utilized [42,43]. Landsat data offers high spatial resolution but has low temporal resolution (revisit period

of 16 days) and is susceptible to cloudy weather, resulting in some missing data and limiting the ability of Landsat data to monitor LUCC [44]. MODIS data feature low spatial resolution but high temporal resolution (revisit period of 8 days), which can be applied to the crop identification and monitoring of large planting areas and single structures [45]. Its characteristics are compatible with the conditions in Northeast China [10,46].

The objectives of this work were to (1) propose a land use classification method applicable to large regional scales; (2) identify the area of each land type and analyze the spatiotemporal changes and drivers of LUCC in Northeast China from 2000 to 2020 and explore the drivers of changes in paddy fields; and (3) analyze trends in paddy fields in future scenarios. These results may provide a reference for securing food, resources and ecological security, and promoting sustainable development.

2. Materials and Methods

2.1. Study Area

The study area is situated in northeastern China, encompassing Heilongjiang, Jilin, and Liaoning Province, as well as the eastern part of the Inner Mongolia Autonomous Region, which includes Hulunbuir, Xing'an League, Tongliao, and Chifeng. It is located between $115^{\circ}05' E \sim 135^{\circ}02' E$ and $38^{\circ}40' N \sim 53^{\circ}34' N$. The total area covers approximately 1.27 million km^2 (Figure 1). This study area has a temperate continental monsoon climate. Summers are mild and humid, while winters are cold and long. Rainfall and warm temperatures coincide in the same season. The annual accumulated temperature is less than 3400°C , and the average annual precipitation is 400–1000 mm, mainly concentrated in the summer from July to September [17]. In most areas, wet and warm conditions can meet the growth needs of rice once a year [18]. Farmland black soil is the predominant soil type in the study area, characterized by its high fertility [47]. This region is characterized by its predominantly flat and extensive topography [48]. It is highly suitable for rice cultivation.

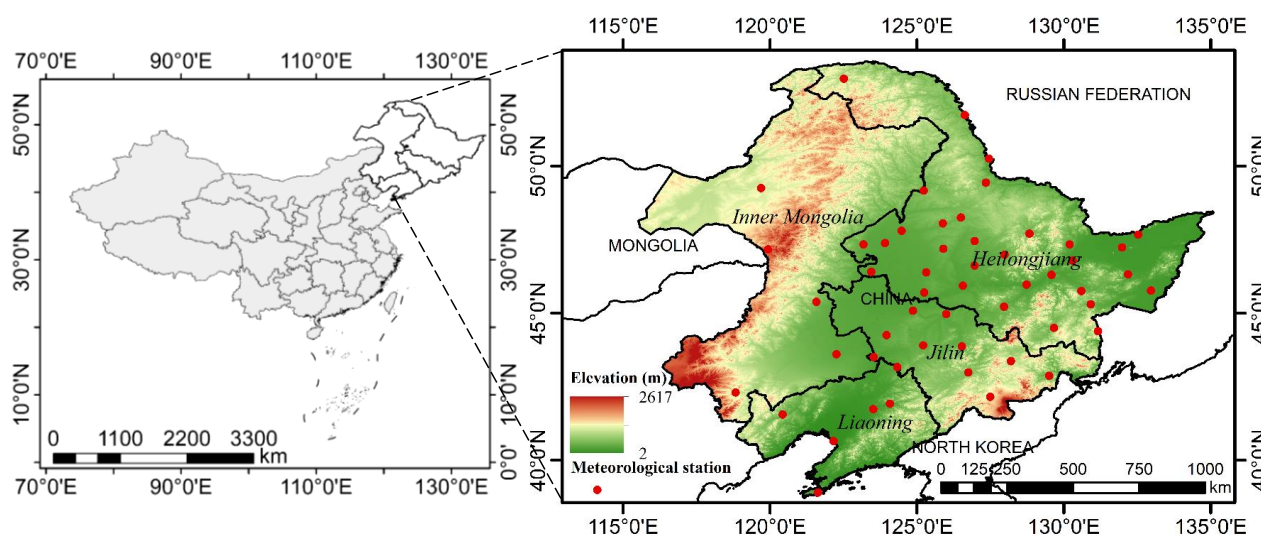


Figure 1. The locations of the China National Meteorological Observatory Stations and study area in Northeast China.

2.2. Datasets

2.2.1. MODIS Data

Global 8-day MODIS products (MOD09A1) with a $500\text{ m} \times 500\text{ m}$ spatial resolution from the United States Geological Survey (USGS) were used in this study, using data from 2000 to 2020. They were acquired from NASA's LPDAAC website: <https://lpdaac.usgs.gov/> (accessed on 23 September 2023). Atmospheric absorption and scattering were removed, and atmospheric correction was carried out. The grid range of the whole region included h25v03, h26v03, h25v04, h26v04, h27v04, and h27v05. The surface reflectance

data included 7 bands as follows: red (620~670 nm), near-infrared (841~876 nm), blue (459~479 nm), green (545~565 nm), thermal infrared (1230~1250 nm), shortwave infrared 1 (1628~1652 nm), and shortwave infrared 2 (2105~2155 nm).

2.2.2. Meteorological Data

The meteorological data utilized in this research were sourced from the China Meteorological Data Network and encompassed the daily average temperature and precipitation recorded at 53 National Meteorological Observatory (NMO) stations between the years 2000 and 2020. Their locations are shown in Figure 1, and they have been meticulously curated and subjected to quality control procedures by the National Climate Information Center, ensuring a data loss rate of under 0.1% [8,49]. In instances where data were sparsely missing, interpolation techniques leveraging information from neighboring stations were employed [50].

2.2.3. CMIP6 Data

The Earth system model is an important tool for comprehending the past and anticipating potential future climate change. The Working Group on Coupled Modeling (WGCM) was established by the World Climate Research Program (WCRP) in 1995 to spearhead and coordinate research efforts. A pivotal development stemming from the WGCM's inception was the initiation of the CMIP [51]. The Scenario Model Comparison Project (Scenario MIP) is a key subproject within CMIP6. It integrates various Representative Concentration Pathways (RCPs) with Shared Socio-economic Pathways (SSPs) to develop its scenarios.

Meteorological projections for future periods are based on the Canadian Earth System Model version 5 (CanESM5), the best climate model selected in CMIP6 for simulating warming trends in northeastern China [52]. Since most CMIP6 models underestimate the multi-year variability in the regional mean temperature and its linear trend, bias correction is needed, and the future climate is predicted based on the bias correction results [53]. The quantile mapping method was applied to bias-correct the temperature data in three different scenarios for the future period of the preferred climate model. The basic assumption is that the difference between the climate model and the observed values for a given quantile during the training period will remain consistent in the future period. The correction method for temperature can be written mathematically as follows [54]:

$$\tilde{x}_{m-p.adjust} = x_{m-p} + (F_{o-c}^{-1}(F_{m-p}(x_{m-p})) - F_{m-c}^{-1}(F_{m-p}(x_{m-p}))) \quad (1)$$

where F represents the cumulative distribution function, F^{-1} represents quantile cumulative distribution function, both of which apply to either observations (o) or model outputs (m) during a historical training period or the current climate (c), as well as the future projection period (p). $\tilde{x}_{m-p.adjust}$ represents the model value after bias correction, and x_{m-p} represents the model value before bias correction.

The climate model data utilized in this study consisted of monthly temperature simulations generated by the CanESM5 global climate model for 2021–2100 from the CMIP6 data. CanESM5 is the current version of the Canadian Centre for Climate Modeling and Analysis's global model, with a resolution of $2.81^\circ \times 2.81^\circ$. There are three scenarios as follows: the low emission scenario SSP1-RCP2.6 (SSP126), the medium emission scenario SSP2-RCP4.5 (SSP245), and the high emission scenario SSP5-RCP8.5 (SSP585). Data were obtained from <https://esgf-node.llnl.gov/search/cmip6> (accessed on 23 September 2023).

2.3. Methods

2.3.1. MODIS Data Preprocessing

The MODIS data from 2000 to 2020 were preprocessed using Environment for Visualizing Images (ENVI), which included coordinate system conversion, data splicing, clipping, and cloud pollution removal. The images were subjected to band operation to obtain the NDVI, EVI, and LSWI spectral indices. Pure pixels were averaged to obtain representative

time series images for various categories, including the Normalized Difference Vegetation Index (NDVI), Land Surface Water Index (LSWI), and Enhanced Vegetation Index (EVI).

The extraction of each land type primarily relies on the phenological characteristics in different periods. Some studies show that the classification accuracy based on the vegetation index is higher than that of other methods [55]. The EVI is not only easily saturated in high biomass areas but can also reduce the influence of background values and atmospheric conditions; it is more suitable for extracting paddy field information. The NDVI is commonly used to assess vegetation growth and coverage, while the LSWI is a normalized index that incorporates the near-infrared and shortwave infrared bands. The shortwave infrared band is particularly responsive to variations in water and can effectively distinguish water, paddy fields, and waterless land. The value range of the LSWI is $[-1, 1]$. The above three indices were calculated by using the band calculation tools in ENVI. The calculation formulas of the EVI, NDVI, and LSWI are as follows [56]:

$$\text{EVI} = 2.5 \times \frac{\rho_{\text{nir}} - \rho_{\text{red}}}{\rho_{\text{nir}} + 6\rho_{\text{red}} - 7.5\rho_{\text{blue}} + L} \quad (2)$$

$$\text{NDVI} = \frac{\rho_{\text{nir}} - \rho_{\text{red}}}{\rho_{\text{nir}} + \rho_{\text{red}}} \quad (3)$$

$$\text{LSWI} = \frac{\rho_{\text{nir}} - \rho_{\text{swir}}}{\rho_{\text{nir}} + \rho_{\text{swir}}} \quad (4)$$

where ρ_{nir} represents the reflectance of the near-infrared channel; ρ_{swir} represents the reflectance of the shortwave thermal infrared channel; ρ_{red} represents the reflectance of the red channel; ρ_{blue} represents the reflectance of the blue channel; and L is the soil regulation parameter, which is set to 1.

2.3.2. Land Use Classification Method

The primary land types in Northeast China include grassland, dry fields, paddy fields, woodland, construction land, water, and unused land. The spectral characteristics and phenological characteristics of these 7 land types are different. According to the features of the study area and its land ecological characteristics, the classification system was established by using the two-grade classification method. Cropland can be subdivided into paddy fields and dry fields, as the phenological characteristics and geographical range vary considerably between the different crop types grown.

Reference pixels were selected for spectral feature analysis, time series curve analysis, and classification accuracy evaluation. A time-consuming and laborious approach involves obtaining the ideal reference pixels through fieldwork. It is simpler and more effective to use high spatial resolution images to validate low spatial resolution images [57]. The visual interpretation of approximately 500 pixels of each of the seven land classes from Google Earth imagery and a comparison with the CLCD data (<http://doi.org/10.5281/zenodo.4417810> (accessed on 23 September 2023)) and Chinese Academy of Sciences (<http://www.resdc.cn> (accessed on 23 September 2023)) classification results was conducted to obtain reference pixels.

The classification method is based on the decision tree algorithm, supplemented by the maximum likelihood method, threshold method, and phenological features [58]. The decision tree uses a top-down recursive approach, using appropriate classification algorithms to create classification nodes and branches based on the spectral characteristics of various land types [59], gradually classifying these various land types. The maximum likelihood method automatically identifies the land class based on the specific time series curve of that land class [60]. The threshold method applies one or more band thresholds to identify a land type based on its band interval characteristics [61,62]. Phenological features are used to identify land types based on the spectral features generated by the growth features of plants.

The classification process was based on multitemporal MODIS images, preprocessed surface reflectance data and vegetation index data, analyzed time-series curves and spectral characteristics according to characteristic variables and surface reflectance bands, a constructed decision tree model, and the output classification results. Finally, the accuracy of the classification results was assessed using the confusion matrix method.

According to the analysis of the spectral features and index time series curves, and after iterative trials, the land use types were extracted according to the following rules:

- (1) Water. The reflectance of the water land type in band 6 on 2 June and 8 October was significantly different than the reflectance of the other land types in band 6. The water body on 8 October was not yet frozen, the surface was not covered by aquatic vegetation, and the water body was clearly visible. Water bodies were extracted using band 6 > 1000 on 2 June and band 6 > 1000 on 8 October.
- (2) Woodland. The EVI for woodland differed significantly from that of the other land types on 25 May and 2 June. Woodland was extracted based on EVI > 0.44 on 25 May or EVI > 0.48 on 2 June.
- (3) Unused land. Unused land has no surface cover, high surface albedo year-round, and low vegetation and moisture indices. It was extracted using a band 6 > 4000 on 7 April, EVI < 0.379 on 12 July, EVI < 0.3488 on 28 July and LSWI < −0.03.
- (4) Paddy field. Referring to Google Maps images from 2000 to 2010, paddy fields were jointly discriminated using band 6 on 2 June and LSWI on 28 July with threshold conditions of <1600 and >0.3, respectively.
- (5) Construction land. The LSWI on 7 April, NDVI on 28 July, LSWI on 8 October, and band 6 on 24 October were used to identify construction land, with values ranging from −0.15 to −0.02, 0.1 to 0.5, −0.1 to 0.1, and 1000 to 2600, respectively.
- (6) Dry field. The LSWI and EVI time series curves of the dry fields were significantly different from those of the grasslands, which were extracted according to the maximum likelihood method.
- (7) Grassland. The remaining pixels were classified as grassland.

2.3.3. Classification Accuracy Verification

According to the above methods and processes, the land in Northeast China from 2000 to 2020 was classified. The period from 2000 to 2010 served as the calibration period, while the period from 2011 to 2020 was used for validation. The calibration period data were used to determine the model threshold of 7 land type classifications, and the validation period data were used to test the time extension of the model. The confusion matrix method was utilized to compare the consistency of the reference pixel classes with the classification results at the same location. Producer accuracy is the proportion of correctly classified elements relative to the total number of elements in the entire image. The kappa coefficient (K) and the total precision (P_o , %) were utilized to determine the accuracy of the classification results [56]. The equations are as follows:

$$P_o = \frac{S}{n} \cdot 100\% \quad (5)$$

$$P_c = \frac{(g_1 \cdot f_1 + g_2 \cdot f_2)}{n^2} \quad (6)$$

$$K = \frac{(P_o - P_c)}{(1 - P_c)} \quad (7)$$

where P_o represents the total precision, indicating the probability that the classification result accurately reflects the actual land use type, %; n represents the total number of pixels in the image; S represents the number of pixels in the same position where the reference pixel land type and the classification result land type agree; P_c is the chance agreement rate, where the probability of the joint occurrence of the two is the product of the probability of the separate occurrence when the classification result is not related to the actual land

use type; g_1 indicates the number of pixels corresponding to a land type in the reference pixel; g_2 indicates the number of pixels corresponding to other land types in the reference pixel; f_1 indicates the number of pixels corresponding to a land type in the classification result; and f_2 indicates the number of pixels corresponding to other land types in the classification result.

2.3.4. Paddy Field Centroid

The centroid method was employed to determine the geographical centroid of paddy fields in Northeast China. The centroid was calculated by averaging the coordinates of each unit of a certain land type. The dynamics of the paddy fields from 2000 to 2020 were obtained from the changes in the centroid. The equations are as follows:

$$X_{k,t} = \frac{\sum_{i=1}^n X_{i,k,t}}{n} \quad (8)$$

$$Y_{k,t} = \frac{\sum_{i=1}^n Y_{i,k,t}}{n} \quad (9)$$

where $X_{k,t}$ represents the longitude and $Y_{k,t}$ represents the latitude of the geographical centroid of land use k , respectively; t represents the year; $X_{i,k,t}$ and $Y_{i,k,t}$ denote the centroid coordinates of pixel i of a certain land use type; and n represents the total number of paddy field pixels.

2.3.5. Quantifying the Impact of Drivers of Paddy Field Area Change

The drivers of paddy field area change in Northeast China can be categorized into three groups, namely, scientific and technological development factors, climatic factors, and policy factors. The contribution of each factor to paddy field area change was quantitatively identified by multiple linear regression methods [63,64]:

$$A_t = \sum_j \alpha_j B_{j,t} + \sum_j \beta_j C_{j,t} + \gamma D_t \quad (10)$$

where A_t represents the area of paddy fields in year t ; $B_{j,t}$ represents the technological development factor, including the total power of agricultural machinery and effective irrigated area in year t , which was obtained from the China National Bureau of Statistics (<https://www.stats.gov.cn/sj/> (accessed on 23 September 2023)); and $C_{j,t}$ represents climatic factors, which consist of average air temperature and annual precipitation. The policy factor D_t is set as a dummy variable, where $D_t = 1$ indicates the presence of favorable policies for paddy field development and $D_t = 0$ indicates the absence of such policies. The estimated parameters are α_j , β_j , and γ .

2.3.6. Climate Change Analysis

Historical temperature changes in Northeast China were analyzed based on the NMO station data. The spatial distribution of annual average temperature in 2000 and 2020 in the study area was derived using kriging spatial interpolation. Kriging was best cross-validated in the study area.

Analysis of future temperature changes in Northeast China and the adjacent regions was based on the CMIP6 data. The future time period is 2021–2100, and the climate change scenarios used were SSP126, SSP245, and SSP585. Trends in annual average temperature change were calculated using trend analysis, and a pixel-by-pixel linear trend analysis was

used to identify trends in annual average temperature variables over a long time series as follows:

$$\text{slope} = \frac{n \times \sum_{j=1}^n j \times X_j - \sum_{j=1}^n j \sum_{j=1}^n X_j}{n \times \sum_{j=1}^n j^2 - \left(\sum_{j=1}^n j \right)^2} \quad (11)$$

where X_j denotes the time series variable, with j denoting the sample series number and t ranging from 1 to n , where n is the total number of years. A *slope* value greater than 0 signifies an upward trend in the corresponding variable, while a *slope* value less than 0 indicates a downward trend. The absolute value of the *slope* reflects the magnitude of the change.

3. Results and Discussion

3.1. Land Use Classification and Accuracy Verification

The time series curves of the NDVI, EVI, and LSWI, drawn according to the reference pixels of seven land types, are shown in Figure 2. In different time intervals, the phenological characteristics and population characteristics were different, and the corresponding spectral characteristics and time series curves were significantly different. Different time intervals exhibit variations in the phenological characteristics and community traits of land use types, which accordingly influence the spectral characteristics and time series curve of indices [65]. For instance, before transplantation, paddy fields are flooded, while post-transplantation, the paddy area consists of both water bodies and seedlings [10]. The spectral characteristics of paddy fields during the transplantation period are unique compared to other land use types. Affected by human or natural factors, the corresponding time series curve fluctuated and changed.

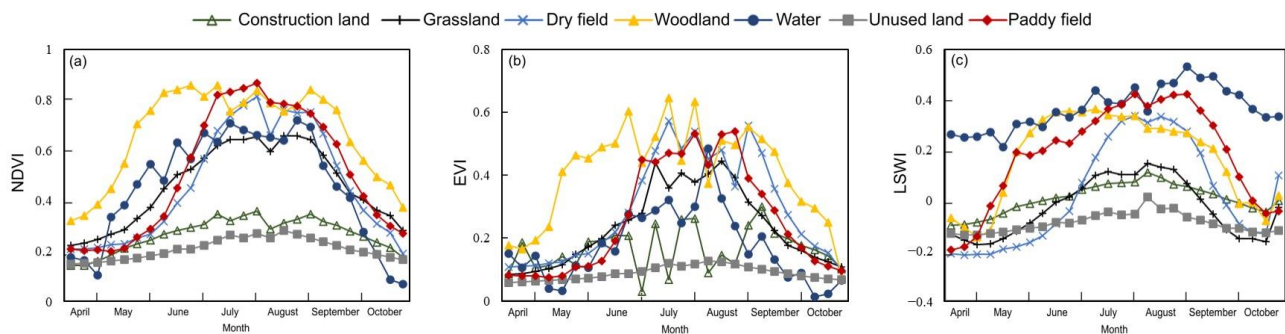


Figure 2. Time series mean curves of three indices under different land use types: (a) NDVI, (b) EVI, and (c) LSWI.

The vegetation had unique spectral characteristics from seedling emergence to mature harvest or wilting, and the corresponding vegetation index time series curve showed a rising and then declining trend. From early April to early June, when the woodlands are in the germination stage and the rice and dry crops are in the transplanting and seedling stages, the NDVI and EVI of the woodlands were notably higher compared to those of other land types, with the maximum differences reaching 0.3 and 0.2, respectively. The LSWI for water was always greater than that for other land types and fluctuated less. Unused land is without any cover year-round, the curve of each index is smooth, the moisture content is lower, the LSWI is significantly smaller than the LSWI of other land types, and the peak fluctuates around 0. Grassland waveforms were similar to those of the woodland, but the indices were low overall. Rice was in the transplanting period from mid-May to early June, as it was irrigated with flooded water, and the LSWI for paddy fields was considerably higher than the LSWI for dry fields, grassland, and construction land, but similar to the LSWI of the water and woodland land types. All indices were lower in construction land,

with a small amount of vegetation cover such as greenery, so the vegetation index was slightly higher than that of unused land.

The confusion matrix was used for accuracy verification, and the classification accuracy evaluation of the calibration period is shown in Table 1. The producer accuracy of the seven types of land from 2000 to 2010 was >0.773 , the accuracy of the woodland type ranged from 0.893 to 0.934, the accuracy of the paddy field type ranged from 0.884 to 0.931, and the overall accuracy varied between 84.3% and 87.3%, while the kappa coefficient ranged from 0.797 to 0.825, which indicated good classification accuracy. The classification accuracy was higher for paddy fields, dry fields, and woodlands, with large areas and concentrated distributions, and lower for grasslands, unused lands, and construction lands, with small areas and fragmented distributions. The reason for this is that there are more mixed pixels in the more fragmented land types, and the presence of mixed pixels reduces the classification accuracy when the basic unit of detection and acquisition of feature information is the pixel [66]. The validity and suitability of different classification rules are different, the maximum likelihood method is sensitive to the sample size and composition, and its classification results will change with the instability of the sample.

Table 1. The evaluation index derived from the confusion matrix from 2000 to 2010.

Year	Producer Accuracy							Overall Accuracy/%	Kappa Coefficient
	Paddy Field	Dry Field	Grassland	Unused Land	Water	Woodland	Construction Land		
2000	0.907	0.881	0.841	0.786	0.865	0.923	0.863	86.0	0.813
2001	0.915	0.873	0.822	0.741	0.906	0.913	0.827	85.6	0.809
2002	0.885	0.885	0.785	0.784	0.875	0.909	0.841	84.3	0.797
2003	0.917	0.884	0.849	0.835	0.827	0.916	0.822	84.9	0.802
2004	0.874	0.831	0.745	0.721	0.844	0.898	0.833	83.9	0.788
2005	0.931	0.897	0.863	0.771	0.891	0.934	0.785	86.4	0.816
2006	0.884	0.906	0.873	0.766	0.894	0.913	0.849	86.7	0.819
2007	0.897	0.911	0.842	0.803	0.891	0.896	0.863	86.5	0.817
2008	0.906	0.905	0.894	0.846	0.862	0.916	0.873	87.3	0.825
2009	0.884	0.886	0.773	0.766	0.894	0.893	0.849	86.7	0.819
2010	0.897	0.891	0.842	0.803	0.801	0.896	0.863	86.5	0.817

The evaluation index of classification accuracy during the validation period is shown in Table 2. The 2011–2020 mapping accuracy for the seven land types was >0.716 , with paddy field accuracy ranging from 0.849 to 0.909, overall accuracy varying between 80.5% and 83.9%, and kappa coefficients varying between 0.761 and 0.793, which basically met the application requirements. Similarly, the classification accuracy was higher for lands with large areas and concentrated distributions (paddy fields, dry fields, and woodlands) and lower for lands with small areas and fragmented distributions (grasslands, unused lands, and construction lands).

Table 2. The evaluation index derived from the confusion matrix from 2011 to 2020.

Year	Producer Accuracy							Overall Accuracy/%	Kappa Coefficient
	Paddy Field	Dry Field	Grassland	Unused Land	Water	Woodland	Construction Land		
2011	0.867	0.875	0.805	0.735	0.871	0.861	0.825	83.9	0.793
2012	0.887	0.853	0.721	0.743	0.833	0.855	0.833	81.4	0.769
2013	0.863	0.865	0.821	0.781	0.832	0.825	0.815	80.5	0.761
2014	0.861	0.835	0.766	0.716	0.799	0.777	0.835	80.8	0.764
2015	0.854	0.867	0.821	0.762	0.767	0.841	0.807	80.8	0.764
2016	0.889	0.881	0.823	0.753	0.815	0.844	0.743	81.6	0.771
2017	0.849	0.834	0.731	0.729	0.844	0.851	0.799	81.7	0.772
2018	0.909	0.871	0.826	0.768	0.846	0.833	0.831	82.3	0.778
2019	0.882	0.858	0.803	0.755	0.815	0.831	0.791	81.3	0.768
2020	0.899	0.854	0.791	0.754	0.856	0.831	0.811	82.0	0.775

3.2. Spatiotemporal Changes in Paddy Fields

The classification results from 2000 to 2020 are shown in Figure 3 (showing one every 2 years). The woodland and dry field types were the largest land types, and the woodland type was primarily distributed in northern Inner Mongolia, the northwest, central, and southeastern regions of Heilongjiang, and the eastern parts of Jilin and Liaoning. The dry field was predominantly found in the central region of the study area and the northeastern part of Heilongjiang Province. Most of the forestland was distributed in the high elevation area, while other land types were located in the plains. Grassland and unused land were mainly distributed in the western part of the study area. It was obvious that some dry fields and grasslands in the northeast were gradually transformed into paddy fields. Due to the farmers' preference for cultivating rice, they have abandoned dryland crops in favor of rice cultivation. The areas of paddy fields, dry fields, and woodlands all showed a continuous upward trend. The most notable change was the expansion of dry fields, followed by that of woodlands and paddy fields. The rates of increase for paddy fields, dry fields, and woodlands were $1.51 \times 10^3 \text{ km}^2/\text{a}$, $4.03 \times 10^3 \text{ km}^2/\text{a}$, and $3.00 \times 10^3 \text{ km}^2/\text{a}$, respectively. The land type with the largest decreasing area was the grassland type, with a decrease of approximately $14.67 \times 10^4 \text{ km}^2$. The spatial change in paddy fields was most obvious from 2000 to 2020, mainly in expansion, especially in the Sanjiang Plain and Songnen Plain of Heilongjiang Province [8]. The woodlands in the northwest of the study area are mixed in the figure, and the main land types resulting in mixing are dry fields and grasslands. There were mixed pixels in the identification of land use types, but the distribution of the seven land types in the study area was continuous and complete, which significantly minimized the effect of mixed pixels on the accuracy of the results.

Northeast China, as a key grain production base, is the country's primary rice-producing region. In particular, rice production in Northeast China has seen rapid growth in recent years. Its contribution to the total output value of grain in China is important. Much attention has been given to the development of rice in Northeast China [16,18,67,68]. Moreover, in recent decades, paddy fields in Northeast China have changed considerably [69].

Changes in paddy fields prior to 2000 have been extensively studied [19,20]. Since 1950, the development of rice has gradually improved. At first, rice cultivation was mainly favored in Liaoning and Jilin. In 1949, Heilongjiang Province had only $1.116 \times 10^5 \text{ ha}$ of rice. In 1985, the technique of dry cultivation and sparse planting of rice was popularized in Heilongjiang Province, resulting in the rapid development of rice cultivation in the whole province. The area used for rice cultivation reached $15.64 \times 10^5 \text{ ha}$ in 1999, representing a 13-fold expansion. Spatially, this area also gradually expanded from the southernmost part to all parts of the province. According to the statistical data, the total rice cultivation area in Northeast China saw minimal change during the 1950s and 1960s. In the 1970s–1980s, paddy field area had a fluctuating growth stage that increased from $8.861 \times 10^5 \text{ ha}$ in 1987 to $16.352 \times 10^5 \text{ ha}$ in 1990, with an average annual growth rate of 5.23% [19]. Rice production in Northeast China has been developing rapidly since 1990. Rapid development has led to a significant change in the regional layout of rice in China. Building on the findings of Gao and Liu [70], Heilongjiang Province experienced an increase in paddy fields by approximately $40,065 \text{ km}^2$ between 1958 and 2018, with $18,461 \text{ km}^2$ of this expansion occurring from 1958 to 2000. As the climate has warmed, rice cultivation has expanded rapidly, pushing the northern boundary up to 52° N [71]. The share of rice production in grain production in the Northeast has also gradually increased, and rice has replaced wheat as the most important grain. Between 1980 and 2010, the rice cultivation area in Northeast China experienced a rapid expansion, increasing by nearly 4.5 times [15]. Meanwhile, the expansion rates of paddy areas were $504 \text{ km}^2/\text{a}$ and $369 \text{ km}^2/\text{a}$ during 1958–1980 and 1980–2000, respectively [72]. The timely updating of land use data in Northeast China is essential. The paddy field area in Northeast China increased by $36.8 \times 10^5 \text{ ha}$ from 2000 to 2017 [18], making this region known as the new “China's bowl” [16].

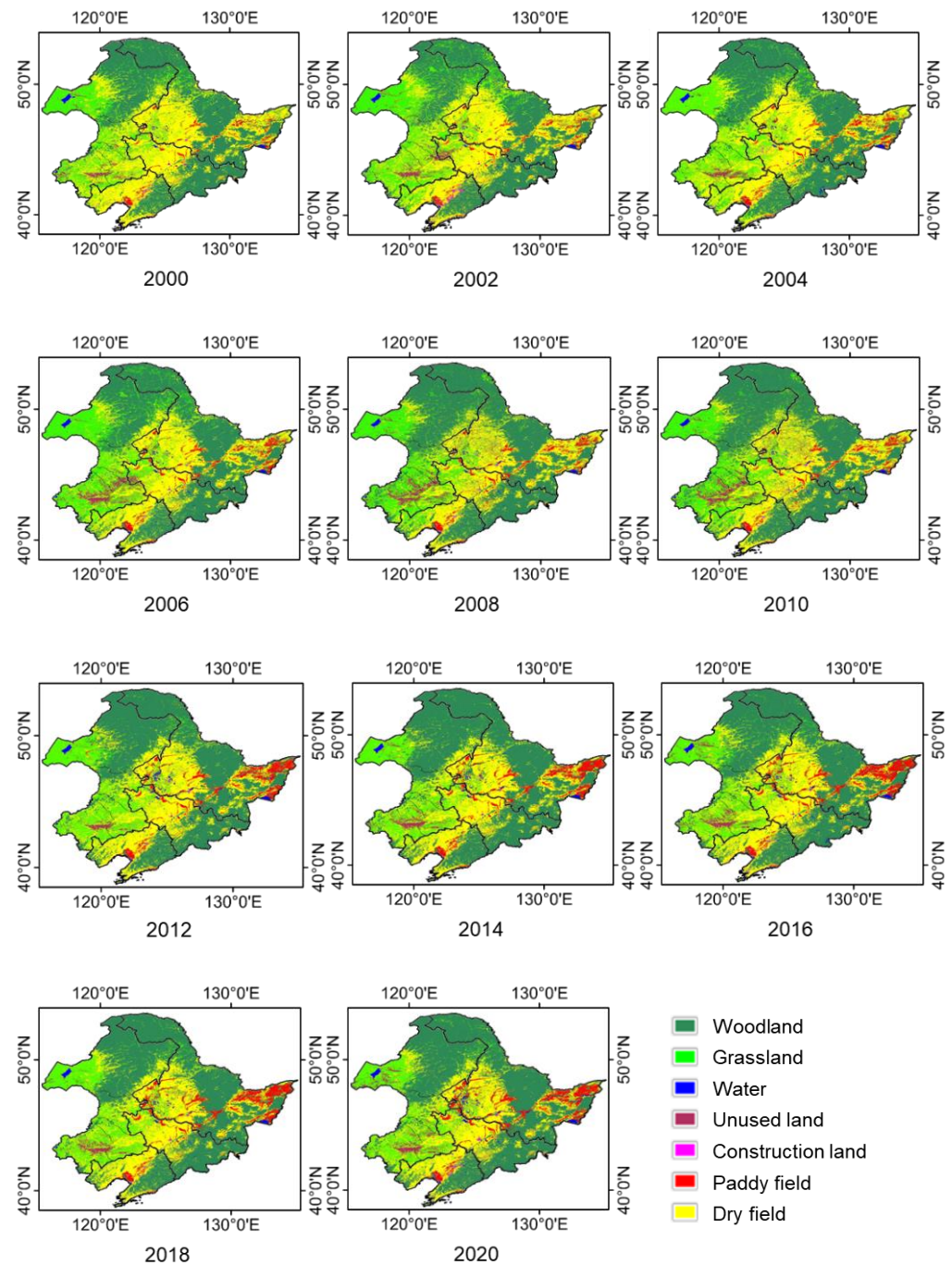


Figure 3. Land use classification results.

The centroids were calculated by averaging the coordinates of each field unit (Figure 4). The centroids of paddy fields and dry fields are distributed in Heilongjiang and Jilin. The centroids of dry fields are relatively concentrated and do not change much. The centroids of the paddy fields showed an obvious banded distribution. They gradually shifted toward the northeast, from Jilin Province to Heilongjiang Province (Figure 5), and the migration distance was 292 km. Before 2010, the centroids were more dispersed and moved farther away; after 2010, they were concentrated and moved less. This indicates that the spatial distribution of paddy fields in the northeast changed rapidly in the first decade and slowed down in the second decade.

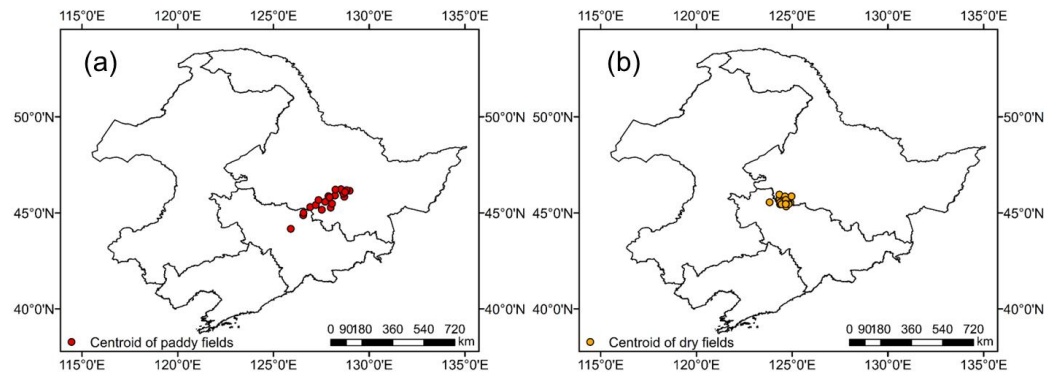


Figure 4. Distribution of the centroids: (a) paddy field; (b) dry field.

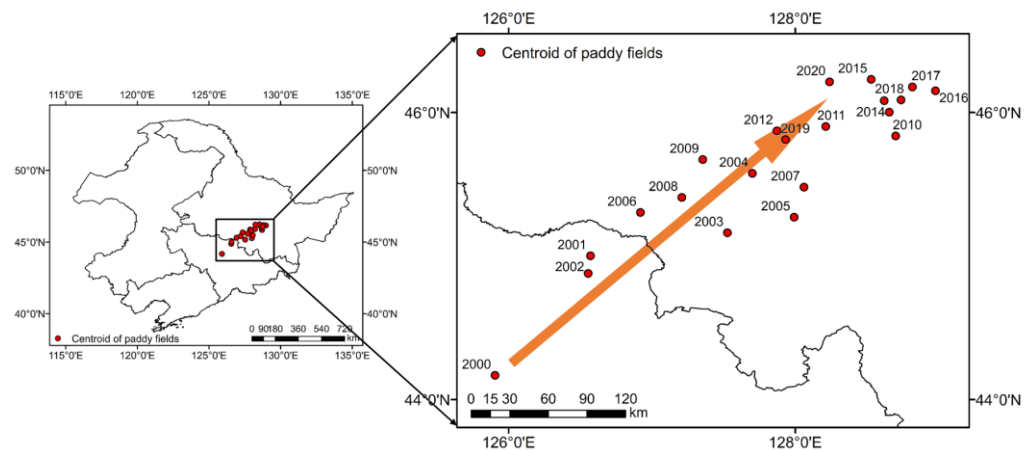


Figure 5. The track of the migration of paddy field centroids.

3.3. Drivers of Paddy Field Change

The reasons behind the expansion of paddy fields are complex. Many scholars have analyzed and studied them. Drivers such as climate change, technology development, farmland policies, and agricultural inputs have been proposed successively. The contributions of each factor were assessed using a multiple linear regression model, with the results presented in Table 3. The total power of agricultural machinery, effective irrigated area, policy support, and average air temperature all positively influenced the area dedicated to rice cultivation, while annual precipitation negatively affected it. Notably, the total power of agricultural machinery and effective irrigated area had a more substantial impact on paddy field area growth, likely because rice cultivation inherently relies on both agricultural machinery and irrigation. Specifically, for every 1% increase in average temperature, the area under rice production increased by nearly 0.02%.

Table 3. Estimated paddy field area function for Northeast China from 2000 to 2020.

Explanatory Variables	Estimated Coefficients	t-Values
Total power of agricultural machinery	0.618	2.202
Effective irrigated area	0.582	1.872
Policy support	0.254	2.770
Average air temperature	0.021	2.298
Annual precipitation	−0.028	−0.465

Climate change plays a crucial role in influencing rice development. Many studies have identified it as the primary driver behind the expansion of rice cultivation. It was proven that climate change, especially temperature increase, greatly affects the changes in paddy field area [15]. Precipitation has not increased significantly during the rice

growth period in recent decades, and it even showed a decreasing trend in Northeast China [72,73]. Rice cultivation in Northeast China primarily relies on groundwater and surface water irrigation rather than precipitation [74]. Therefore, the expansion of paddy fields in Northeast China is not closely related to regional precipitation changes [15]. Past studies have proven that temperature fluctuations increased in Northeast China from 1950 to 2020. The increase in temperature provided more heat resources for crop production. Rice growth duration also improved and shortened in response to climate change. Climate warming in Northeast China has expanded the paddy field area and caused significant changes in the cropping structure of food crops. In the past 30 years, the cumulative temperature in the northeast has increased, and the cumulative temperature zone has shifted northward and eastward. The annual average temperature decline trend at the centroid is $0.0454\text{ }^{\circ}\text{C/a}$, which is less than the annual average temperature decline trend associated with the latitude (Figure 6). Climate warming has eased the constraints of cooler northern temperatures on the northward migration of paddy fields. The temperature in Northeast China is gradually rising. As shown in Figure 7, the high-temperature area expanded from 2000 to 2020, and the isotherms moved northward. Climate warming in the northeast cold region was a major reason for the northward shift in the rice planting centroid [70,75].

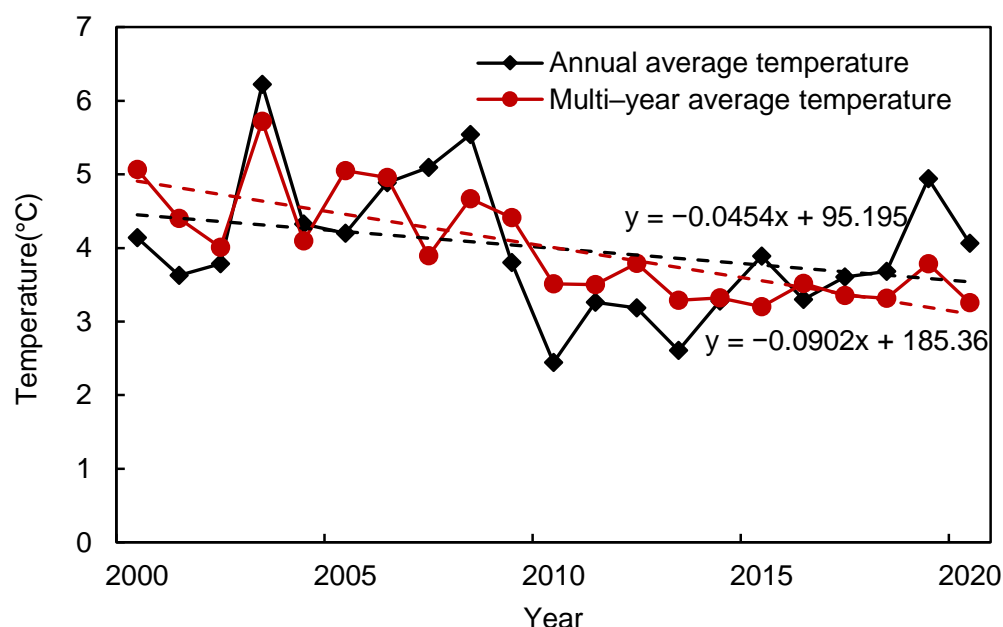


Figure 6. Annual average temperature and multi-year average temperature in different centroids.

Additionally, the techniques of greenhouse seedling raising and well water temperature heightening have been gradually popularized, reducing chilling injury in rice seedlings, which is another main reason for the expansion of paddy fields. The continuous improvement of rice farming technology is another important factor for the development of rice in cold regions [76]. Regarding seedling planting, Jilin and Heilongjiang have focused on the promotion of dry seedling technology in greenhouses, while Liaoning has mainly experimented with the promotion of nonwoven fabric cover insulation seedling technology. With the continuous improvement and popularization of greenhouse seedling cultivation and well water warming technologies, frost damage to rice seedlings has been reduced. In the transplanting link, Jilin and Heilongjiang promoted sparse planting and super sparse planting technology. Drought and water-saving cultivation techniques were also suggested. For example, in Jilin Province, comprehensive water-saving and drought-resistant cultivation techniques were vigorously promoted, and in Liaoning Province, drought-resistant and water-saving techniques such as dry seedlings, dry land preparation and intermittent irrigation were promoted, which eased the pressure on water resources [71]. Rice produc-

tion mechanization has also developed quickly. In 2006, the integrated mechanization rate of field operations in Heilongjiang Reclamation reached 92%, more than 50% higher than that of the whole country. The expansion of rice cultivation has been supported by the development of cultivation techniques, particularly against chilling injury [77,78].

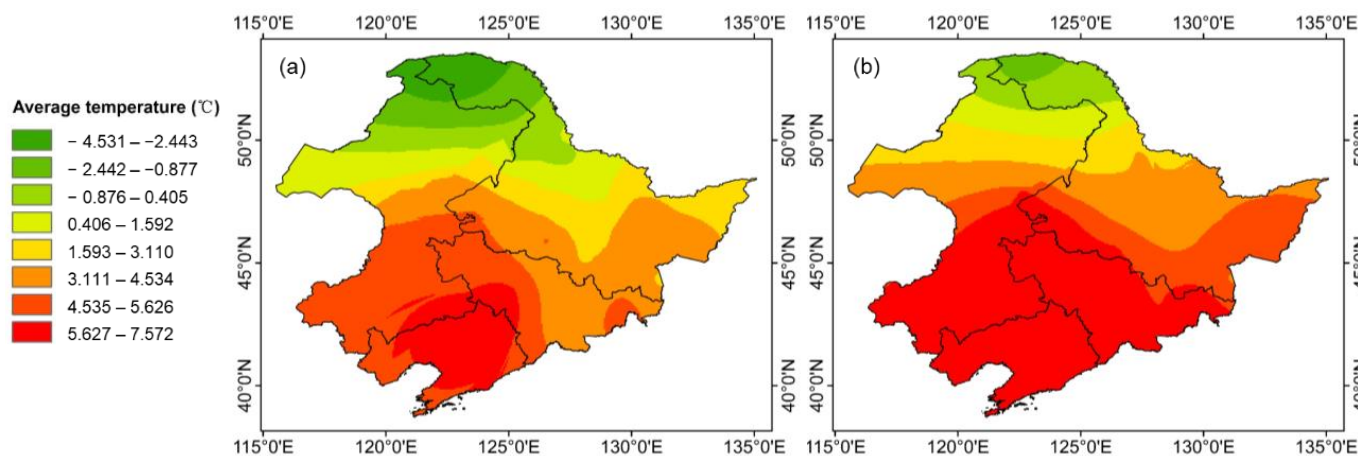


Figure 7. Spatial distribution of annual average temperature in Northeast China: (a) 2000, (b) 2020.

To bolster national food security, China's central government has introduced a range of policies in Heilongjiang that offer economic incentives and preferential policies for agricultural development and farmland preservation. These measures have encouraged local governments and farmers to actively participate in land reclamation and crop cultivation [78,79]. Since 1979, the state has significantly increased the purchase price of grain, resulting in an increase in the price of rice in the Northeast region. The benefits of rice cultivation are higher than those of dry crops [80,81]. Moreover, many people in China believe that rice from Northeast China tastes better and there is less concern about soil and water contamination than rice from southern China, which has contributed to the higher profitability and expansion of paddy fields in Northeast China [82]. Farmers have a stronger willingness to cultivate rice with policy and market support.

3.4. Prediction of Future Paddy Fields Under Future Climate Scenarios

The conditions that need to be met for rice to grow include water, heat, and space. Rice cannot be cultivated in areas with low annual average temperatures [27]. Northeast China was too cold to grow rice before the 1980s [83,84]. However, the above discussion shows that the paddy boundary is gradually moving to the northeast as the climate warms, so it is possible that rice will continue to develop to the northeast and even cross the Russian–Chinese border and grow in the southern part of Far East Russia due to climate change. The future temperature change in Northeast China from 2021 to 2100 was analyzed based on the bias correction results of the CMIP6 data (Figure 8) to determine whether it can reach the suitable temperature of 10–38 °C for rice growth [85]. The latest transplanting period for rice in Northeast China generally occurs in May. If the temperature in May reaches 11.5 °C, the rice growth requirements can be met [86]. In this study, it was determined that the temperature conditions required for rice cultivation were satisfied if the local average temperature in May steadily exceeded 11.5 °C (greater than 11.5 °C for five consecutive years), and the site was considered a potentially suitable area for rice cultivation (Figure 9).

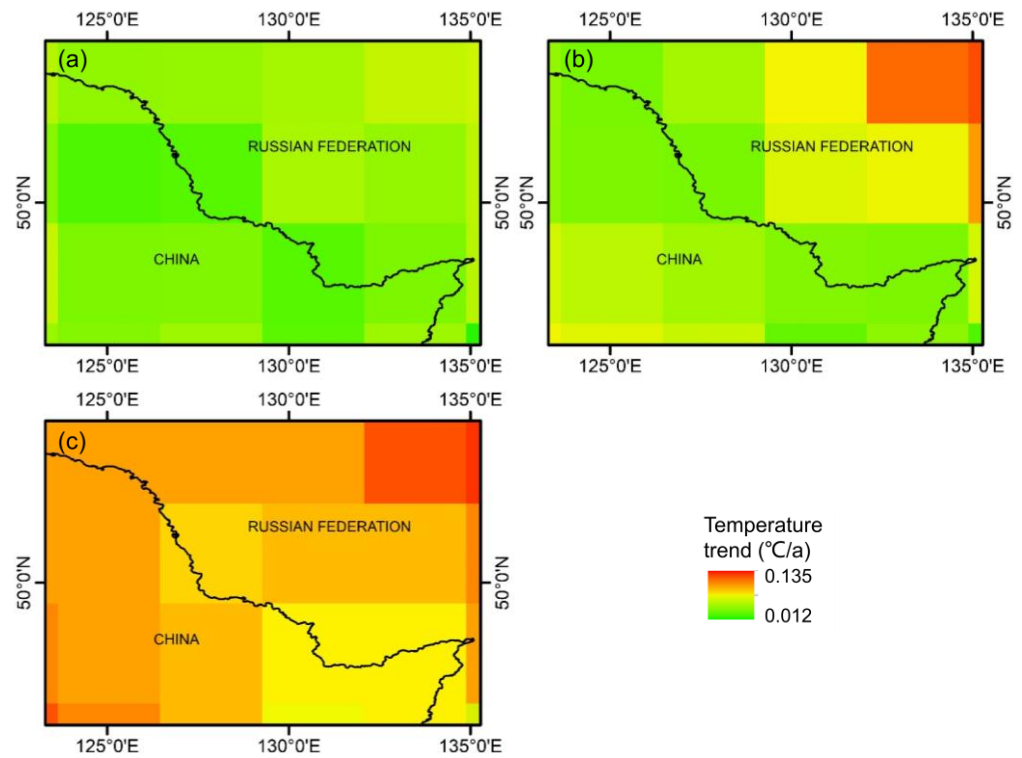


Figure 8. Trend of average temperature in May from 2021 to 2100 under future scenarios: (a) SSP126, (b) SSP245, and (c) SSP585.

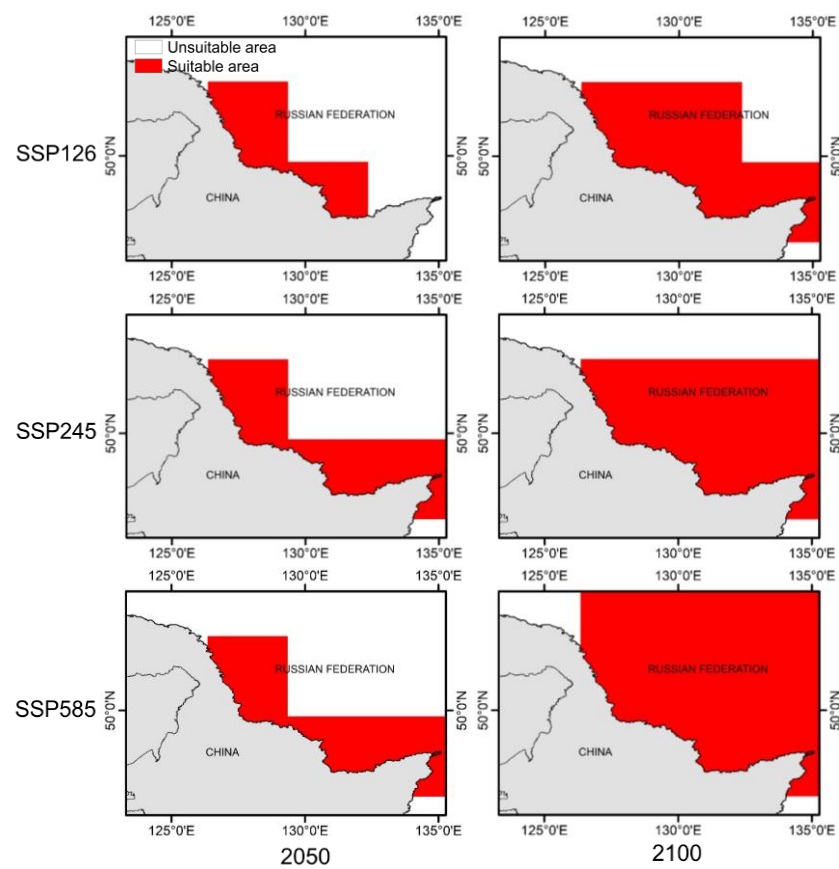


Figure 9. Temperature-suitable area for rice cultivation in 2050 and 2100 under SSP126, SSP245, and SSP585.

According to the results, the average temperature in Northeast China and most of its surrounding areas will continue to rise under the three scenarios of SSP126, SSP245, and SSP585 in 2021–2100. The climate in the Far East Russia border with Northeast China will gradually warm, with a significant upward trend in average temperatures. Under the SSP126 scenario, the average temperature in most regions shows an upward trend. The temperature will increase fastest in the Far East Russia border with Northeast China, reaching $0.021\text{ }^{\circ}\text{C}/\text{a}$. The temperature in May will reach a maximum of $13.26\text{ }^{\circ}\text{C}$ in 2100, which just meets the temperature conditions for rice growth [22]. The area that achieves the temperature requirement for rice growth will be small until 2050 in Far East Russia, and the suitable growth area for rice will increase by 2100. Under the SSP245 scenario, the increase in temperature will be fastest in Far East Russia and in the northeastern border region of Northeast China, reaching $0.065\text{ }^{\circ}\text{C}/\text{a}$. The annual average temperature in May could reach $16.40\text{ }^{\circ}\text{C}$ in 2100, which meets the temperature conditions for rice growth. In 2050, there will be some areas that meet the requirements for rice cultivation, and in 2100, the areas of Far East Russia near Northeast China will basically meet them. Under the SSP585 scenario, the fastest rate of temperature increase in the northeast and the surrounding regions is $0.104\text{ }^{\circ}\text{C}/\text{a}$. In 2100, the May average temperature in Far East Russia could reach $20.38\text{ }^{\circ}\text{C}$, which will completely meet the temperature conditions for rice growth. Due to the rapid increase in temperature, Far East Russia will have many areas near China that could meet the temperature requirements for rice growth by 2100. The potential suitable area for rice cultivation is the largest in the SSP585 scenario. The area suitable for rice cultivation under the three scenarios tends to expand to the northeast in 2021–2100. The higher the future emissions are, the larger the potentially suitable area for rice planting in 2100. Therefore, Far East Russia will likely meet the temperature conditions for growing rice in the future, and paddy fields can be developed if water and land resources are sufficient. There exists the potential to continue the development of rice cultivation from China to the northeast.

4. Conclusions

Land use and land cover in Northeast China has changed considerably. MODIS remote sensing data were used to identify land use types from 2000 to 2020 through the decision tree method and to analyze the main land type changes. The future development trend of paddy fields from 2021 to 2100 was also explored based on the temperature predicted by the CMIP6 climate model.

A decision tree model was constructed based on the phenological features of each land type to identify the spatiotemporal distribution of each land type in Northeast China. The overall accuracy in the calibration period ranged from 84.3% to 87.3%, and the kappa coefficient ranged from 0.797 to 0.825. The overall accuracy during the validation period varied between 80.5% and 83.9%, and the kappa coefficient ranged from 0.761 to 0.793.

LUCC in Northeast China is dominated by the expansion of woodlands, paddy fields, and dry fields, with the area of grasslands gradually decreasing. Among them, paddy fields show a gradual northward shift, with the centroids gradually shifting toward the northeast. Paddy fields are mainly transformed from dry fields. Woodlands and dry fields are mainly converted from grasslands.

The expansion of paddy fields in Northeast China is influenced by several factors. The natural factor is the warming climate that meets the necessary growth conditions for rice. Technological factors include the continuous progress in rice planting techniques, such as the gradual improvement and expansion of local well water heating and greenhouse rice growing techniques. The social factor is the strong support of the national government in terms of policy.

According to the future temperature under different scenarios of CMIP6, the temperature in Far East Russia and northern Northeast China will gradually rise. These areas will thus meet the temperature conditions for rice growth in SSP126, SSP245, and SSP585. Under the SSP585 scenario, the temperature will rise the fastest, and the area suitable for rice cultivation will be the largest. Therefore, the climatic conditions for the continuous

northward movement of paddy fields will be met. It will be possible to grow rice in Far-East Russia in the future.

Author Contributions: Conceptualization, Y.L. and X.H.; methodology, Y.C.; software, P.H., D.Y. and Y.W.; validation, D.Y.; investigation, Y.X., C.S. and Y.W.; data curation, X.H.; formal analysis, C.S., writing—original draft preparation, X.H.; writing—review and editing, Y.L. and P.H.; visualization, Y.X.; supervision, Y.C. All authors have read and agreed to the published version of the manuscript.

Funding: This study was financially supported by the National Natural Science Foundation of China (52379046 and 51979201) and the Water Resources S&T Project of Inner Mongolia Autonomous Region, China (No. NSK 2021-01).

Institutional Review Board Statement: Not applicable.

Data Availability Statement: Data are contained within the article.

Acknowledgments: The observed meteorological data were sourced from the China Meteorological Data Sharing Service System (<http://data.cma.cn/> (accessed on 23 September 2023)), the MODIS images were sourced from USGS (<https://lpdaac.usgs.gov/> (accessed on 23 September 2023)), the CMIP6 data were sourced from World Climate Research Programme (<https://esgf-node.llnl.gov/search/cmip6> (accessed on 23 September 2023)), and the land use information was provided by the Institute of Remote Sensing Information Processing, Wuhan University (<http://doi.org/10.5281/zenodo.4417810> (accessed on 23 September 2023)) and Data Center for Resources and Environmental Sciences, Chinese Academy of Sciences (<http://www.resdc.cn> (accessed on 23 September 2023)), which we gratefully acknowledge. We also would like to thank the editor and the three anonymous reviewers for their insightful comments.

Conflicts of Interest: Author Changhong Song was employed by the company Heilongjiang Water Conservancy Investment Group Co., Ltd. The remaining authors declare that the research was conducted in the absence of any commercial or financial relationships that could be construed as a potential conflict of interest.

References

1. Valbuena, D.; Verburg, P.H.; Bregt, A.K. A method to define a typology for agent-based analysis in regional land-use research. *Agric. Ecosyst. Environ.* **2008**, *128*, 27–36. [[CrossRef](#)]
2. Yan, D.; Schneider, U.A.; Schmid, E.; Huang, H.Q.; Pan, L.; Dilly, O. Interactions between land use change, regional development, and climate change in the Poyang Lake district from 1985 to 2035. *Agric. Syst.* **2013**, *119*, 10–21. [[CrossRef](#)]
3. Deng, G.; Jiang, H.; Zhu, S.; Wen, Y.; He, C.; Wang, X.; Sheng, L.; Guo, Y.; Cao, Y. Projecting the response of ecological risk to land use/land cover change in ecologically fragile regions. *Sci. Total Environ.* **2024**, *914*, 169908. [[CrossRef](#)] [[PubMed](#)]
4. Lang, Y.; Song, W. Quantifying and mapping the responses of selected ecosystem services to projected land use changes—ScienceDirect. *Ecol. Indic.* **2019**, *102*, 186–198. [[CrossRef](#)]
5. Meyfroidt, P.; Lambin, E.F.; Erb, K. Globalization of land use: Distant drivers of land change and geographic displacement of land use. *Curr. Opin. Environ. Sustain.* **2013**, *5*, 438–444. [[CrossRef](#)]
6. Deng, L.; Liu, G.; Shangguan, Z. Land-use conversion and changing soil carbon stocks in China’s ‘Grain-for-Green’ Program: A synthesis. *Glob. Change Biol.* **2014**, *20*, 3544–3556. [[CrossRef](#)]
7. Xiang, X.; Zhai, Z.; Fan, C.; Ding, Y.; Ye, L.; Li, J. Modelling future land use land cover changes and their impacts on urban heat island intensity in Guangzhou China. *J. Environ. Manag.* **2024**, *366*, 121787. [[CrossRef](#)]
8. Hu, X.; Chen, M.; Liu, D.; Li, D.; Jin, L.; Liu, S.; Cui, Y.; Dong, B.; Khan, S.; Luo, Y. Reference evapotranspiration change in Heilongjiang Province, China from 1951 to 2018: The role of climate change and rice area expansion. *Agric. Water Manag.* **2021**, *253*, 106912. [[CrossRef](#)]
9. Liu, C.; Xu, Y.; Lu, X. Spatio-temporal evolution and optimization regionalization of trade-off and synergy of land use functions in ecologically fragile and poverty areas: A case study of Zhangjiakou City. *Econ. Geography* **2021**, *41*, 181–190. (In Chinese with English Abstract).
10. Xiao, X.; Boles, S.; Froking, S. Mapping paddy rice agriculture in South and Southeast Asia using multi-temporal MODIS images. *Remote Sens. Environ.* **2006**, *100*, 95–113. [[CrossRef](#)]
11. Wang, J.; Zhang, Z.; Liu, Y. Spatial shifts in grain production increases in China and implications for food security. *Land Use Policy* **2018**, *74*, 204–213. [[CrossRef](#)]
12. Wang, Y.; Hu, X.; Wei, B.; Luo, Z.; Wang, Z.; Chen, C. Assessing landscape ecological risk in the Southern Hill and Mountain Belt of China: A 30-year analysis and future projection. *Ecol. Indic.* **2024**, *166*, 112283. [[CrossRef](#)]
13. Wang, B.; Oguchi, T.; Liang, X. Evaluating future habitat quality responding to land use change under different city compaction scenarios in Southern China. *Cities* **2023**, *140*, 104410. [[CrossRef](#)]

14. Hu, J.; Wu, Y.; Wang, L.; Sun, P.; Zhao, F.; Jin, Z.; Wang, Y.; Lian, Y. Impacts of land-use conversions on the water cycle in a typical watershed in the southern Chinese Loess Plateau. *J. Hydrol.* **2021**, *593*, 125741. [[CrossRef](#)]
15. Xia, T.; Wu, W.; Zhou, Q. Spatio-temporal changes in the rice planting area and their relationship to climate change in Northeast China: A model-based analysis. *J. Integr. Agric.* **2014**, *13*, 1575–1585. [[CrossRef](#)]
16. Liu, Y.; Liu, X.; Liu, Z. Effects of climate change on paddy expansion and potential adaption strategies for sustainable agriculture development across Northeast China. *Appl. Geogr.* **2022**, *141*, 102667. [[CrossRef](#)]
17. Cao, D.; Feng, J.; Bai, L.; Xun, L.; Jing, H.; Sun, J.; Zhang, J. Delineating the rice crop activities in Northeast China through regional parametric synthesis using satellite remote sensing time-series data from 2000 to 2015. *J. Integr. Agric.* **2021**, *20*, 424–437. [[CrossRef](#)]
18. Xin, F.; Xiao, X.; Dong, J.; Zhang, G.; Zhang, Y.; Wu, X.; Li, X.; Zou, Z.; Ma, J.; Du, G.; et al. Large increases of paddy rice area, gross primary production, and grain production in Northeast China during 2000–2017. *Sci. Total Environ.* **2020**, *711*, 135183. [[CrossRef](#)]
19. Tong, C.; Hall, C.A.; Wang, H. Land use change in rice, wheat and maize production in China (1961–1998). *Agric. Ecosyst. Environ.* **2003**, *95*, 523–536. [[CrossRef](#)]
20. Gao, J.; Liu, Y.; Chen, Y. Land cover changes during agrarian restructuring in Northeast China. *Appl. Geogr.* **2006**, *26*, 312–322. [[CrossRef](#)]
21. Tian, J.; Wang, B.; Zhang, C.; Li, W.; Wang, S. Mechanism of regional land use transition in underdeveloped areas of China: A case study of Northeast China. *Land Use Policy* **2020**, *94*, 104538. [[CrossRef](#)]
22. Yang, F.Y.; Zheng, Q.H.; Luo, J.M. *Practical Agrometeorological Indicators*; China Meteorological Press: Beijing, China, 2015. (In Chinese with English Abstract).
23. García-Álvarez, D.; Olmedo, M.T.C.; Delden, H.V.; Mas, J.F.; Paegelow, M. Comparing the structural uncertainty and uncertainty management in four common Land Use Cover Change (LUCC) model software packages. *Environ. Modell. Softw.* **2022**, *153*, 105411. [[CrossRef](#)]
24. Wang, H.; Stephenson, S.R.; Qu, S. Modeling spatially non-stationary land use/ cover change in the lower Connecticut River Basin by combining geographically weighted logistic regression and the CA-Markov model. *Int. J. Geogr. Inf. Sci.* **2019**, *33*, 1313–1334. [[CrossRef](#)]
25. Mahiny, A.S.; Clarke, K.C. Simulating hydrologic impacts of urban growth using SLEUTH, multi criteria evaluation and runoff modeling. *J. Environ. Inf.* **2013**, *22*, 27–38. [[CrossRef](#)]
26. Saxena, A.; Jat, M.K. Land suitability and urban growth modeling: Development of SLEUTH-Suitability. *Comput. Environ. Urban Syst.* **2020**, *81*, 101475. [[CrossRef](#)]
27. Li, X.; Lin, J.; Chen, Y.; Liu, X.; Ai, B. Calibrating cellular automata based on landscape metrics by using genetic algorithms. *Int. J. Geogr. Inf. Sci.* **2013**, *27*, 594–613. [[CrossRef](#)]
28. Aburas, M.M.; Ho, Y.M.; Ramli, M.F.; Ashaari, Z.H. Improving the capability of an integrated CA-Markov model to simulate spatio-temporal urban growth trends using an Analytical Hierarchy Process and Frequency Ratio. *Int. J. Appl. Earth Obs. Geoinf.* **2017**, *59*, 65–78. [[CrossRef](#)]
29. Yue, W.; Qin, C.; Su, M.; Teng, Y.; Xu, C. Simulation and prediction of land use change in Dongguan of China based on ANN cellular automata-Markov chain model. *Environ. Sustain. Indic.* **2024**, *22*, 100355. [[CrossRef](#)]
30. Liu, X.P.; Liang, X.; Li, X.; Xu, X.C.; Ou, J.P.; Chen, Y.M.; Li, S.Y.; Wang, S.J.; Pei, F.S. A future land use simulation model (FLUS) for simulating multiple land use scenarios by coupling human and natural effects. *Landsc. Urban Plan* **2017**, *168*, 94–116. [[CrossRef](#)]
31. Saeedi, S. Integrating macro and micro scale approaches in the agent-based modeling of residential dynamics. *Int. J. Appl. Earth Obs. Geoinf.* **2018**, *68*, 214–229. [[CrossRef](#)]
32. Basse, R.M.; Omrani, H.; Charif, O.; Gerber, P.; Bódis, K. Land use changes modelling using advanced methods: Cellular automata and artificial neural networks. The spatial and explicit representation of land cover dynamics at the cross-border region scale. *Appl. Geogr.* **2014**, *53*, 160–171. [[CrossRef](#)]
33. Tong, X.; Feng, Y. A review of assessment methods for cellular automata models of land-use change and urban growth. *Int. J. Geogr. Inf. Sci.* **2020**, *34*, 866–898. [[CrossRef](#)]
34. Hu, Y.; Fan, L.; Liu, Z.; Yu, Q.; Liang, S.; Chen, S.; You, L.; Wu, W.; Yang, P. Rice production and climate change in Northeast China: Evidence of adaptation through land use shifts. *Environ. Res. Lett.* **2019**, *14*, 024014. [[CrossRef](#)]
35. National Bureau of Statistics of China. *China Statistical Yearbook*; Statistics Press: Beijing, China, 2023. (In Chinese)
36. Salma, S.; Keerthana, N.; Dodamani, B.M. An optimum datasets analysis for monitoring crops using remotely sensed Sentinel-1A SAR data. *Int. J. Remote Sens.* **2023**, *44*, 4372–4391. [[CrossRef](#)]
37. Fensholt, R.; Langanke, T.; Rasmussen, K.; Reenberg, A.; Prince, S.D.; Tucker, C.; Scholes, R.J.; Le, Q.B.; Bondeau, A.; Eastman, R.; et al. Greenness in semi-arid areas across the globe 1981–2007: an Earth Observing Satellite based analysis of trends and drivers. *Remote Sens. Environ.* **2012**, *121*, 144–158. [[CrossRef](#)]
38. Gimenez, R.; Laloue, A.; Fabre, S. Rejection methods for vegetation mapping using hyperspectral airborne data. *Int. J. Remote Sens.* **2023**, *44*, 4937–4962. [[CrossRef](#)]
39. Simonneaux, V.; Duchemin, B.I.T.; Helson, D. The use of high-resolution image time series for crop classification and evapotranspiration estimate over an irrigated area in central Morocco. *Int. J. Remote Sens.* **2008**, *29*, 95–116. [[CrossRef](#)]
40. Wang, Y.; Sun, Y.; Cao, X.; Wang, Y.; Zhang, W.; Cheng, X. A review of regional and Global scale Land Use/Land Cover (LULC) mapping products generated from satellite remote sensing. *Isprs. J. Photogramm.* **2023**, *206*, 311–334. [[CrossRef](#)]

41. Tucker, C.J.; Townshend, J.R.G. African land cover classification using satellite data. *Science* **1985**, *227*, 369–375. [[CrossRef](#)]
42. Lu, M.; Chen, J.; Tang, H.; Rao, Y.; Yang, P.; Wu, W. Land cover change detection by integrating object-based data blending model of Landsat and MODIS. *Remote Sens. Environ.* **2016**, *184*, 374–386. [[CrossRef](#)]
43. Buchner, J.; Yin, H.; Frantz, D.; Kuemmerle, T.; Askerov, E.; Bakuradze, T.; Bleyhl, B.; Elizbarashvili, N.; Komarova, A.; Lewińska, K.E.; et al. Land-cover change in the Caucasus Mountains since 1987 based on the topographic correction of multi-temporal Landsat composites. *Remote Sens. Environ.* **2020**, *248*, 111967. [[CrossRef](#)]
44. Piedadlobo, L.; Hernández-López, D.; Ballesteros, R.; Chakhar, A.; Pozo, S.D.; González-Aguilera, D.; Moreno, M.A. Scalable pixel-based crop classification combining Sentinel-2 and Landsat-8 data time series: Case study of the Duero river basin. *Agric. Syst.* **2019**, *171*, 36–50. [[CrossRef](#)]
45. Zeng, T.; Zhang, Z.; Zhao, X.; Wang, X.; Zuo, L. Evaluation of the 2010 MODIS collection 5.1 land cover type product over China. *Remote Sens.* **2015**, *7*, 1981–2006. [[CrossRef](#)]
46. Ba, S.; Wang, W.J.; Sun, H.; Bao, S.G.; Zhang, H.; He, H.S. The cooling and warming effects of potential forest transition on local land surface temperature in Northeast China. *Ecol. Indic.* **2024**, *159*, 111645. [[CrossRef](#)]
47. Luo, C.; Zhang, W.; Meng, X.; Yu, Y.; Zhang, X.; Liu, H. Mapping the soil organic matter content in Northeast China considering the difference between dry lands and paddy fields. *Soil Tillage Res.* **2024**, *244*, 106270. [[CrossRef](#)]
48. Zhao, W.; Hu, W.; Zhang, F.; Shi, Y.; Wang, Y.; Zhang, X.; Feng, T.; Hong, Z.; Jiang, J.; Xu, R. Exchangeable acidity characteristics of farmland black soil in northeast China. *Geoderma Reg.* **2024**, *38*, e00852. [[CrossRef](#)]
49. Zhao, Z.; Wang, H.; Wang, C.; Li, W.; Chen, H.; Deng, C. Changes in reference evapotranspiration over Northwest China from 1957 to 2018: Variation characteristics, cause analysis and relationships with atmospheric circulation. *Agric. Water Manag.* **2020**, *231*, 105958. [[CrossRef](#)]
50. Lin, P.F.; He, Z.B.; Du, J.; Chen, L.F.; Zhu, X.; Li, J. Impacts of climate change on reference evapotranspiration in the Qilian Mountains of China: Historical trends and projected changes. *Int. J. Climatol.* **2018**, *38*, 2980–2993. [[CrossRef](#)]
51. Meehl, G.A.; Boer, G.J. Intercomparison makes for a better climate model. *Eos. Trans. Am. Geophys. Union* **1997**, *78*, 445–451. [[CrossRef](#)]
52. He, X.; Jiang, C.; Wang, J.; Wang, X. Comparison of CMIP6 and CMIP5 models performance in simulating temperature in Northeast China. *Chinese. J. Geophys.-Chin.* **2022**, *202*, 4194–4207, (In Chinese with English Abstract).
53. He, C.; Luo, C.; Chen, F.; Long, A.; Tang, H. Prediction of future climate change in Hotan River Basin Based on CMIP6 multi model. *Earth Sci. Front.* **2023**, *30*, 1–14. (In Chinese with English Abstract).
54. Li, H.; Sheffield, J.; Wood, E.F. Bias correction of monthly precipitation and temperature fields from Intergovernmental Panel on Climate Change AR4 models using equidistant quantile matching. *J. Geophys. Res. Atmos.* **2010**, *2010*, 115. [[CrossRef](#)]
55. Gong, P. Vegetation Classification Based on Phenology Indices Derived from MODIS Data in Northeastern China. *Resour. Sci.* **2010**, *2010*, 1154–1160.
56. Chen, Y.; Li, D.; Li, Z.; Chen, M.; Cui, Y.; Luo, Y. Rice planting area extraction based on multi-temporal MODIS images in Heilongjiang Province of China. *Trans. Chin. Soc. Agric. Eng.* **2020**, *36*, 201–208. (In Chinese with English Abstract).
57. Sun, Y.; Yang, X.; Wang, X. Land use classification based on decision tree using MODIS data. *Resour. Sci.* **2007**, *29*, 169–174, (In Chinese with English Abstract).
58. Liu, J.; Li, L.; Huang, X. Mapping paddy rice in Jiangsu province, China, based on phenological parameters and a decision tree model. *Front. Earth Sci.* **2019**, *13*, 111–123. [[CrossRef](#)]
59. Otukei, J.R.; Blaschke, T. Land cover change assessment using decision trees, support vector machines and maximum likelihood classification algorithms. *Int. J. Appl. Earth Obs.* **2010**, *12*, S27–S31. [[CrossRef](#)]
60. Shivakumar, B.R.; Rajashekararadhya, S.V. Investigation on Land Cover Mapping Capability of Maximum Likelihood Classifier: A Case Study on North Canara, India. *Procedia Comput. Sci.* **2018**, *143*, 579–586. [[CrossRef](#)]
61. Neinavaz, E.; Andrew, K.; Skidmore, A.; Roshanak, D. Effects of prediction accuracy of the proportion of vegetation cover on land surface emissivity and temperature using the NDVI threshold method. *Int. J. Appl. Earth Obs.* **2020**, *85*, 101984. [[CrossRef](#)]
62. Shao, Q.; Zhang, W.; Cao, X.; Yang, J.; Yin, J. Threshold and moderating effects of land use on metro ridership in Shenzhen: Implications for TOD planning. *J. Transp. Geogr.* **2020**, *89*, 102878. [[CrossRef](#)]
63. Kutner, M.H.; Nachtsheim, C.J.; Neter, J.; Li, W. *Applied Linear Statistical Models*, 5th ed.; McGraw-Hill Irwin: New York, NY, USA, 2005.
64. Montgomery, D.C.; Runger, G.C. *Applied Statistics and Probability for Engineers*, 7th ed.; Wiley: Hoboken, NJ, USA, 2018.
65. Peng, D.; Huete, A.R.; Huang, J. Detection and estimation of mixed paddy rice cropping patterns with MODIS data. *Int. J. Appl. Earth Obs. Geoinf.* **2011**, *13*, 13–23. [[CrossRef](#)]
66. Fatholouloumi, S.; Firozjaei, M.K.; Li, H.; Biswas, A. Surface biophysical features fusion in remote sensing for improving land crop/cover classification accuracy. *Sci. Total Environ.* **2022**, *838*, 156520. [[CrossRef](#)] [[PubMed](#)]
67. Jiang, Y.; Lu, Z.; Li, S.; Lei, Y.; Chu, Q.; Yin, X.; Chen, F. Large-scale and high-resolution crop mapping in China using Sentinel-2 satellite imagery. *Agriculture* **2020**, *10*, 433. [[CrossRef](#)]
68. Liu, W.; Dong, J.; Du, G.; Zhang, G.; Hao, Z.; You, N.; Zhao, G.; Flynn, K.; Yang, T.; Zhou, Y. Biophysical effects of paddy rice expansion on land surface temperature in Northeastern Asia. *Agric. For. Meteorol.* **2022**, *315*, 108820. [[CrossRef](#)]
69. Wang, X.; Li, T.; Yang, X.; Zhang, T.; Liu, Z.; Guo, E.; Lai, Y. Rice yield potential, gaps and constraints during the past three decades in a climate-changing Northeast China. *Agric. For. Meteorol.* **2018**, *259*, 173–183. [[CrossRef](#)]

70. Gao, J.; Liu, Y. Climate warming and land use change in Heilongjiang Province, Northeast China. *Appl. Geogr.* **2011**, *31*, 476–482. [[CrossRef](#)]
71. Yun, Y.R.; Fang, X.Q.; Qiao, D.F.; Wang, Y. Main grain crops structure change in Heilongjiang Province of China in the past 20 years. In Proceedings of the 2005 IEEE International Geoscience and Remote Sensing Symposium, 2005, IGARSS'05, Seoul, Republic of Korea, 29 July 2005; Volume 4, pp. 2858–2861.
72. Wang, B.; Zhang, M.; Wei, J.; Wang, S.; Li, X.; Li, S.; Zhao, A.; Li, X.; Fan, J. Changes in extreme precipitation over Northeast China, 1960–2011. *Quatern. Int.* **2013**, *298*, 177–186. [[CrossRef](#)]
73. Wang, W.; Yin, S.; Yu, J.; He, Z.; Xie, Y. Long-term trends of precipitation and erosivity over Northeast China during 1961–2020. *Int. Soil Water Conserv. Res.* **2023**, *11*, 743–754. [[CrossRef](#)]
74. Zhang, Q.; Sun, J.; Dai, C.; Zhang, G.; Wu, Y. Sustainable development of groundwater resources under the large-scale conversion of dry land into rice fields. *Agric. Water Manag.* **2024**, *298*, 108851. [[CrossRef](#)]
75. Lu, Z.; Song, Q.; Liu, K.; Wu, W.; Liu, Y.; Xin, R.; Zhang, D. Rice cultivation changes and its relationships with geographical factors in Heilongjiang Province, China. *J. Integr. Agric.* **2017**, *16*, 2274–2282. [[CrossRef](#)]
76. Yan, F.; Yu, L.; Yang, C.; Zhang, S. Paddy field expansion and aggregation since the mid-1950s in a cold region and its possible causes. *Remote Sens.* **2018**, *10*, 384. [[CrossRef](#)]
77. Huang, P.; Xie, H.; Yang, Y.; Hu, X.; Liu, C.; Xu, Y.; Song, C.; Dai, C.; Khan, S.; Cui, Y.; et al. Spatiotemporal variation in rice water requirements and area in the cold rice cultivation region of China: Past and Future. *Agric. Water Manag.* **2024**, *298*, 108858. [[CrossRef](#)]
78. Sudu, B.; Li, K.; Guga, S.; Gele, T.; Zhi, F.; Guo, Y.; Wei, S.; Rong, G.; Bao, Y.; Liu, X.; et al. Index construction and real-time hazard assessment of rice sterile-type chilling injury process in Northeast China. *Agric. For. Meteorol.* **2024**, *353*, 110070. [[CrossRef](#)]
79. Zhang, W.Q.; Song, G. Spatial-temporal variations and driving factor analysis of paddy fields in typical regions of Sanjiang Plain. *Trans. Chin. Soc. Agric. Eng.* **2019**, *35*, 244–252. (In Chinese with English Abstract).
80. Chen, H.; Meng, F.; Yu, Z.; Tan, Y. Spatial-temporal characteristics and influencing factors of farmland expansion in different agricultural regions of Heilongjiang Province, China. *Land Use Policy* **2022**, *115*, 106007. [[CrossRef](#)]
81. Pan, T.; Du, G.; Dong, J.; Kuang, W.; De Maeyer, P.; Kurban, A. Divergent changes in cropping patterns and their effects on grain production under different agro-ecosystems over high latitudes in China. *Sci. Total Environ.* **2019**, *659*, 314–325. [[CrossRef](#)]
82. Hansen, J.; Fuller, F.; Gale, F.; Crook, F.; Wailes, E.; Moore, M. China's Japonica Rice Market: Growth and Competitiveness. In *Rice Situation and Outlook Yearbook*; Economic Research Service: Washington, DC, USA, 2001.
83. Li, Z.; Liu, Z.; Anderson, W.; Yang, P.; Wu, W.; Tang, H.; You, L. Chinese rice production area adaptations to climate changes, 1949–2010. *Environ. Sci. Technol.* **2015**, *49*, 2032–2037. [[CrossRef](#)] [[PubMed](#)]
84. Tang, P.; Yang, P.; Chen, Z.; Liu, Z. The impact of climate change on rice spatial distribution in the Northeast China Plain. In Proceedings of the 2012 IEEE First International Conference on Agro-Geoinformatics (Agro-Geoinformatics), Shanghai, China, 2–4 August 2012; pp. 1–4.
85. Song, Y.; Wang, C.; Linderholm, H.W.; Fu, Y.; Cai, W.; Xu, J.; Zhuang, L.; Wu, M.; Shi, Y.; Wang, G.; et al. The negative impact of increasing temperatures on rice yields in southern China. *Sci. Total Environ.* **2022**, *820*, 153262. [[CrossRef](#)]
86. Li, W.; Chen, S.; Yang, H. Temperature conditions and rice planting in the Hongxinglong area of Heilongjiang reclamation area. *Mod. Agric.* **2004**, *2004*, 1–3. (In Chinese)

Disclaimer/Publisher's Note: The statements, opinions and data contained in all publications are solely those of the individual author(s) and contributor(s) and not of MDPI and/or the editor(s). MDPI and/or the editor(s) disclaim responsibility for any injury to people or property resulting from any ideas, methods, instructions or products referred to in the content.